Energy & Environmental Science

Accepted Manuscript

ROYAL SOCIETY OF CHEMISTRY

www.rsc.org/ees

Energy & Environmental Science

ARTICLE

Development of Novel Lithium Borate Additives for Designed Surface Modification of High Voltage $LiNi_{0.5}Mn_{1.5}O_4$ Cathodes

Received 00th January 20xx,
Accepted 00th January 20xx

DOI: 10.1039/x0xx00000x

www.rsc.org/

Mengqing Xu, [a] Liu Zhou, [a] Yingnan Dong, [a] Yanjing Chen, [a] Julien Demeaux, [a] Alex D. Mac Intosh, [a] Arnd Garsuch, [b] and Brett L. Lucht [a,*]

A novel series or lithium alkyl trimethyl borates and lithium aryl trimethyl borates have been prepared and investigated as cathode film forming additives. The borates are prepared via the reaction of lithium alkoxides or lithium phenoxides with trimethyl borate. Incorporation of 0.5-2.0 % (wt) of the lithium borates to a baseline electrolyte (1.0 M $LiPF_6$ in 3:7 (EC/EMC)) results in improved capacity retention and efficiency of high voltage graphite / $LiNi_{0.5}Mn_{1.5}O_4$ cells especially upon cycling at elevated temperature (55 °C). The improved performance results from the sacrificial oxidation of the lithium borate on the cathode surface to generate a cathode passivation film. The lithium borates can be readily structurally modified to act as a functional group delivery agent to modify the cathode surface. Ex-situ surface analysis of the electrodes after cycling confirms that the lithium borates modify the cathode surface and generate a borate rich surface film which inhibits electrolyte oxidation and Mn dissolution.

Introduction

Lithium ion batteries are widely used for portable electronics and are currently being incorporated into electric vehicles due to high gravimetric and volumetric energy density.[1,2] However, cycle life, calendar life, and energy density are some of the major obstacles to the widespread use of lithium-ion batteries in vehicle applications.[3] In an effort to achieve higher energy density, significant effort has been directed to expand the operating potential of the cathode material. Most commercial lithium ion batteries contain lithium transition metal oxide cathode materials, including layered $LiCoO_2$ and spinel $LiMn_2O_4$. These materials are typically charged to ~4.0 V or below vs. Li/Li^+.[3] Cathode materials with a potential over 4.2 V (vs Li/Li^+) have been developed, including $LiMnPO_4$,[4–6] $LiNiPO_4$ [5,7–9] $LiCoPO_4$, [10–12] and $LiNi_{0.5}Mn_{1.5}O_4$.[13–16] Among these promising new cathodes, $LiNi_{0.5}Mn_{1.5}O_4$ has attracted the most attention in recent years because of the high intercalation/deintercalaition potential of 4.8 V (vs. Li/Li^+) and excellent rate performance. However, a major difficulty in using these high-voltage materials is the instability of the standard electrolyte, $LiPF_6$, in organic carbonate solvents, with the cathode surface at operating potentials over 4.5 V. [3,17–20]

Various methods have been proposed to inhibit the detrimental reactions of the electrolyte on the surface of the high voltage cathode materials. One method involves the incorporation of inert surface coatings, such as Al_2O_3, ZnO, and Bi_2O_3 to prevent the oxidation of the electrolyte.[13,14,21,22] However, this strategy has problems related to imperfect surface coatings, difficulty in scale up for commercial applications, and involves additional processing cost. Alternatively, since the oxidative stability of the state-of-art electrolyte, $LiPF_6$ in carbonate solvents, is reported to be limited by the oxidative stability of the organic carbonate solvents, there has been significant interest in development of novel organic solvents with high anodic stability. Sulfones, lactones, organic nitriles, and fluorinated carbonates have been reported to be stable over 5 V (vs. Li/Li^+). However, alternative solvents have problems associated with high viscosity, instability at low potentials, lack of formation of a protective solid electrolyte interface (SEI) on the graphite anode, or high cost. Finally, there have been additional investigations of the incorporation of cathode film forming additives which are sacrificially oxidized on the cathode surface to generate a cathode passivation layer.[22–32] The use of additives to generate a stable cathode passivation layer is similar in nature to the incorporation of electrolyte additives such as vinylene carbonate (VC) and propane sultone (PS) which generate a superior anode SEI. [33–35] The use of electrolyte additives is an easily incorporated solution to the instability of the electrolyte at high potential.

The failure mechanisms of $LiNi_{0.5}Mn_{1.5}O_4$ cells at high voltage and elevated temperature have been recently investigated.[36,37]

[a] Department of Chemistry, University of Rhode Island, Rhode Island 02881, USA.
[b] BASF SE, GCN/E, Ludwigshafen am Rhein 67056, Germany.
* E-mail: blucht@chm.uri.edu

It has been reported that the leading sources of performance loss include solvent oxidation on the cathode surface and transition metal dissolution facilitated by acidic species which result from the thermal or hydrolytic decomposition of $LiPF_6$.[38] Several reports on the improvement of the performance of $Li/LiNi_{0.5}Mn_{1.5}O_4$ cells and graphite/$LiNi_{0.5}Mn_{1.5}O_4$ cells via incorporation of cathode film forming additives have emerged over the past few years.[22–32] Reported additives include 5-hydroxy-1*H*-indazole, phosphite-derivatives, lithium difluoro(oxalato)borate, and lithium bis(oxalato)borate. Each of the additives has been reported to improve the capacity retention and cycle life of graphite/ $LiNi_{0.5}Mn_{1.5}O_4$ cells. Among these additive, lithium bis(oxalato)borate (LiBOB) has been extensively investigated due to multiple benefits in the battery system. The oxidation of LiBOB on the charged $LiNi_{0.5}Mn_{1.5}O_4$ surface at high voltages (> 4.5 V, vs. Li/Li^+) results in the generation of a borate containing surface film along with CO_2 gas evolution.[39] The presence of the borate rich surface film passivates the surface of the $LiNi_{0.5}Mn_{1.5}O_4$ inhibiting capacity loss and Mn dissolution. Unfortunately, LiBOB does not improve cell efficiency.

There is significant interest in the development of novel cathode film forming additives which improve the cycling performance of graphite/ $LiNi_{0.5}Mn_{1.5}O_4$ cells. In an effort to develop novel additives which passivate the $LiNi_{0.5}Mn_{1.5}O_4$ surface, a novel class of lithium aryl trimethyl borates and lithium alkyl trimethyl borates has been developed. The reaction of the lithium phenoxides or lithium alkoxides with trimethyl borate affords a series of lithium borates which can act as functional group delivery agents (Scheme 1). The functionalized anionic additives are electron rich species which are attracted to the cathode upon cell polarization increasing the concentration of the reactive species at the cathode surface.[40] The functionalized borates can contain unsaturated groups for polymerization, Lewis basic groups to inhibit $LiPF_6$ decomposition,[41,42] trimethyl silyl groups, or a range of other functional groups. Reaction of the functionalized lithium borates is designed to generate a borate rich surface with designed organic functionality to stabilize the $LiNi_{0.5}Mn_{1.5}O_4$/electrolyte interphase at high voltage and elevated temperature. Electrochemical methods and ex-situ analysis have been used to understand the role of lithium aryl trimethyl borates and lithium alkyl trimethyl borates in the enhanced performance of graphite/$LiNi_{0.5}Mn_{1.5}O_4$ cells. The novel electrolyte system utilizes Additives for Designed Surface Modification (ADSM) to generate a cathode passivation layer similar in nature to the Solid Electrolyte Interphase (SEI) on the anode.

Scheme 1

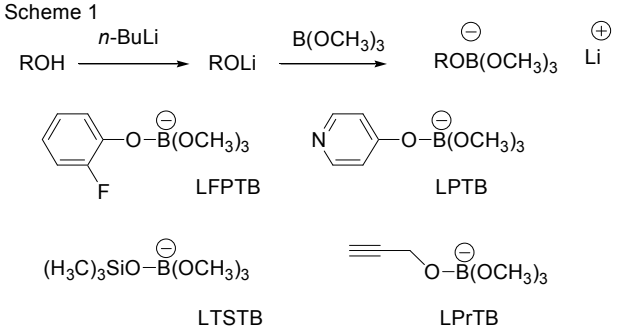

Experimental

Synthesis and characterization

All manipulations were carried out using standard vacuum, Schlenk, cannula, or glovebox techniques. All chemicals were purchased from Aldrich, Fisher, or Strem and used as received unless otherwise noted. ^1H, ^{13}C, ^{11}B, and ^{19}F spectra were recorded on a Bruker Avance 300 MHz spectrometer. Lithium alkyl trimethyl and lithium aryl trimethyl borates were prepared via reaction of the corresponding lithium alkoxide or lithium aryloxide with one equiv. trimethyl borate in THF (Scheme 1). All compounds are synthesized in the same manner. In a 250 mL Schlenk flask, one equiv. (0.02 mol) of the alkyl or aryl alcohol are dissolved in 100 mL of THF and cooled in an ice water bath under N_2. Next, 12.5 mL (0.02 mol) of *n*-BuLi was slowly added with stirring and slowly warmed to room temperature over the course of an hour. The white precipitate that formed was collected via filtration, washed with THF, and dried *in vacuo*. The isolated salt was suspended in 20 mL of THF and slowly added to a solution of one equiv. trimethyl borate with stirring at room temperature. After addition, the solution was stirred at room temperature for one day. The white precipitate was isolated via filtration, washed with diethyl ether followed by dimethyl carbonate and dried *in vacuo*. The product was characterized by ^1H, ^{11}B, and ^{13}C NMR spectroscopy. See the Supplemental Material for the NMR spectra of the lithium borates.

Lithium 2-fluorophenol trimethyl borate (LFPTB). Yield 72%. ^1H NMR (23 °C, D_2O): δ 3.20 (s, 9H, -OCH_3), 6.48 (m, 1H, *aryl*), 6.71 (m, 1H, *aryl*), 6.80 (m, 1H, *aryl*), 6.91 (m, 1H, *aryl*). ^{13}C NMR (23 °C, D_2O): δ 49.53 (-OCH_3), 116.1, 119.95, 124.63, 150.60, 152.34, 156.06 (*aryl*). ^{11}B NMR (23 °C, D_2O): δ 12.12. ^{19}F NMR (23 °C, D_2O): δ -137.77.

Lithium 4-pyridyl trimethyl borate (LPTB). Yield 82%. ^1H NMR (23 °C, D_2O): δ 3.18 (s, 9H, -OCH_3), 6.38 (d, 6.0 Hz, 2H, *aryl*), 7.75 (d, 6.0 Hz, 2H, *aryl*). ^{13}C NMR (23 °C, D_2O): δ 48.76 (-OCH_3), 116.30, 143.73, 177.74 (*aryl*). ^{11}B NMR (23 °C, D_2O): δ 1.82.

Lithium trimethylsilyl trimethyl borate (LTSTB). Yield: 68%. ^1H NMR (23 °C, D_2O): δ 0.08 (s, 9H, -CH_3), 3.29 (s, 9H, -OCH_3). ^{11}B NMR (23 °C, D_2O): δ 2.14.

Lithium propargyl trimethyl borate (LPrTB). Yield 78%. ^1H NMR (23 °C, D_2O): δ 3.20 (s, 9H, -OCH_3), 4.08 (s, 2H, -CH_2), 4.69 (s, 1H, -C*H*). ^{11}B NMR (23 °C, D_2O): δ 2.40.

Electrolyte preparation

Battery grade carbonate solvents, ethylene carbonate (EC) and ethyl methyl carbonate (EMC) and Lithium

hexafluorophosphonate ($LiPF_6$) were provided by BASF. The baseline electrolyte is 1.0 M $LiPF_6$ EC/EMC (3/7, v/v). Electrolytes containing (0.5%, 1.0%, or 2.0% (wt.)) of the lithium borates were prepared from the baseline electrolyte for further evaluations.

Cell construction and cycling protocol

Composite $LiNi_{0.5}Mn_{1.5}O_4$ cathode electrodes were provided by BASF and contain active material (92%), conductive carbon (4%) and PVDF binder (4%). Composite anode electrodes were provided by BASF and consist of graphite (ConocoPhilips,

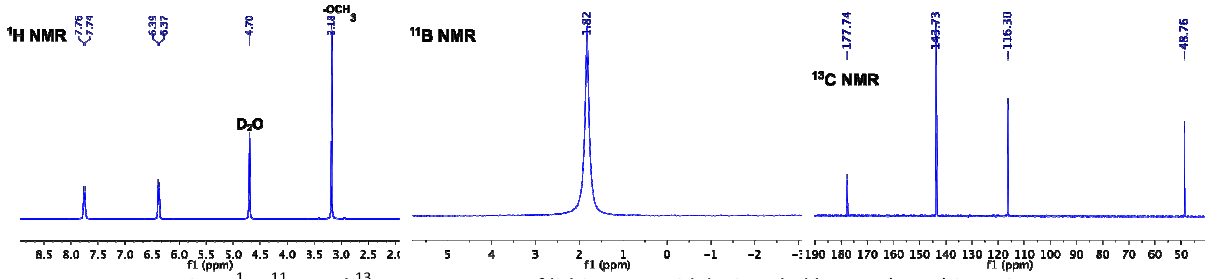

Fig. 1 ^{1}H, ^{11}B, and ^{13}C NMR spectra of lithium 4-pyridyl trimethyl borate (LPTB) in D_2O.

95.7%) along with conductive carbon (0.5%) and CMC & SBR binder (3.8%). Graphite/$LiNi_{0.5}Mn_{1.5}O_4$ 2025-type coin cells were assembled in argon glovebox and for electrochemical performance measurements with trilayer polypropylene/polyethylene (PP/PE/PP) separator (Celgard).

The graphite/$LiNi_{0.5}Mn_{1.5}O_4$ cells were cycled at room temperature with the following cycling protocol, C/20 for the first cycle; C/10 for the second and third cycle; C/5 for the remaining cycles, for a total of 16 cycles at room temperature (RT, 25 ^{o}C). After RT cycling, the cells were transferred to an elevated temperature (ET, 55 ^{o}C) oven and cycled at a C/5 rate for 30 cycles to simulate accelerated aging of the cells. The cells were then returned to RT for another 20 cycles at C/5 rate. The cells were charged with constant current (CC) to 4.8 V followed by constant voltage (CV) (V=4.8 V, vs. Li/Li^+) until the current decreases to 10% of the applied charging current for all cycles. The cells were discharged to 4.25 V with the same constant current (CC). The coin cells were sealed with epoxy resin prior to transfer to an oven (55 ^{o}C). There was no evidence for cell leakage after cycling at ET. Cells were built in triplicate. Cell to cell variation was less than 5%. Representative cycling data is provided. Cell to cell reproducibility with the baseline electrolyte is presented in the Supplementary Information (Fig. S1).

Ex-surface analysis of the electrodes

The cycled cells were disassembled in an argon glove-box, and the cycled anodes/cathodes were harvested and rinsed with anhydrous dimethyl carbonate (DMC) 3 x 1 mL to remove residual $LiPF_6$ and EC, followed by vacuum drying overnight at room temperature. Surface morphology of the cycled electrodes was characterized by scanning electron microscopy (FE-SEM, Zeiss Sigma). For TEM analysis, the cycled electrodes were exposed to ultrasound in DMC solvent for 3h to allow homogenous dispersion of the active materials in the solution, and then the dispersed solution was cast on a copper TEM grid (500 mesh) and dried overnight in a vacuum oven. The TEM grids were quickly transferred into the TEM chamber. Imaging was conducted using a JEOL JEM-2100F TEM (Perbody, MA) at 160 eV. Energy-dispersive X-ray spectroscopy or EDX (model INCAx-act, Oxford Instrument, UK) was used to detect the element composition at various points on the surface and in the bulk material of the particles. The diameter of the beam was 5 nm, and low-dose imaging was employed to minimize electron-beam-induced changes to organic components in the surface layer.

X-ray photoelectron spectroscopy (XPS) was performed on a PHI 5500 system using Al Ka radiation (hv=1486.6 eV) under ultrahigh vacuum conditions. Lithium was not monitored due to its low inherent sensitivity and small change of binding energy. Calibration of XPS peak position was made by recording XPS spectra for reference compounds, which are present on the electrode surface: LiF, PVDF, and $Li_xPO_yF_z$. The graphite peak at 284.3 eV was used as a reference for the final adjustment of the energy scale in the spectra. The spectra obtained were analyzed by Multipack 6.1 A software. Line syntheses of elemental spectra were conducted using Gaussian-Lorentzian (80:20) curve fitting. Elemental concentration was calculated based on the equation: $C_x=(I_x/S_x)/(\sum Ix/Sx)$, where I_x is the relative intensity of the element, and S_x is the sensitivity value of the element. The FTIR spectra were acquired on Bruker Tensor 27 with Attenuated Total Reflectance (ATR) accessory with Germanium crystal, 256 scans with the resolution of 4 cm^{-1}. Samples for XPS and IR analysis were handled under air free conditions.

Results and discussion

Synthesis and characterization of lithium alkyl trimethyl and lithium aryl trimethyl borates

Lithium alkyl trimethyl and lithium aryl trimethyl borates are prepared via the reaction of lithium alkoxides or lithium phenoxides with trimethyl borate in THF. The products precipitate as white powders and are purified via washing with diethyl ether followed by dimethyl carbonate. The white powders are dried in vacuum. The isolated products are purified via crystallization. The compounds have been characterized via NMR spectroscopy, ^{1}H, ^{11}B, and ^{13}C, in D_2O.

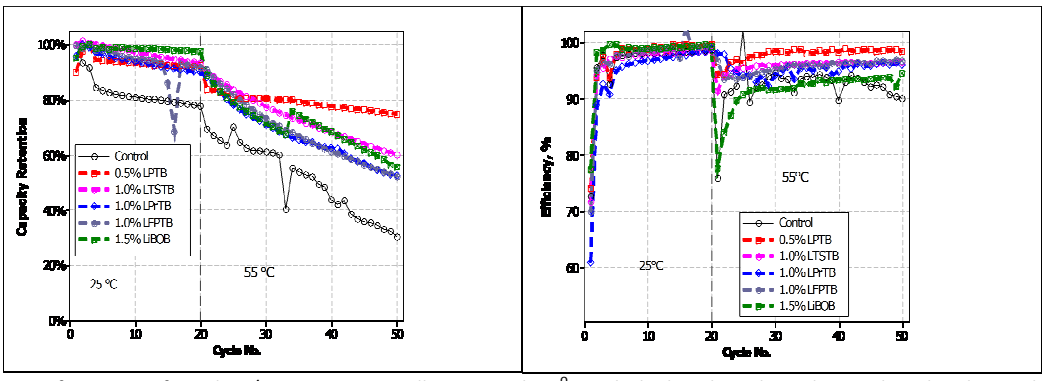

Fig. 2 Cycling performance of graphite/ $LiNi_{0.5}Mn_{1.5}O_4$ cells at 25 and 55 °C with the baseline electrolyte with and without added lithium 4-pyridyl trimethyl borate (LPTB).

Representative ^{1}H, ^{11}B, and ^{13}C NMR spectra of lithium 4-pyridyl trimethyl borate are depicted in Fig. 1. The singlet at 3.18 ppm is characteristic of the methoxy group ($-OCH_3$) in the product, while the singlet at 4.70 ppm is characteristic of the residual H_2O in D_2O. Two doublets are observed at 6.3 and 7.7 ppm and are attributed to two sets of aromatic protons. Integration of the peaks provides the ratio of 2:2:9, for the set of aromatic peaks and the methyl peaks, respectively, as expected for the product. The ^{13}C NMR spectrum provides additional support for a single pure compound with peaks at 48.76, 116.30, 143.73, and 177.74 ppm, respectively, corresponding to the methoxy group ($-OCH_3$), and carbons on the aromatic ring, respectively. A single peak characteristic of the product was observed at 1.82 ppm in the ^{11}B NMR spectrum. The ^{1}H, ^{11}B, and ^{13}C NMR spectra are consistent with lithium 4-pyridyl trimethyl borate of high purity (> 99 %).

Cycling performance of graphite/$LiNi_{0.5}Mn_{1.5}O_4$ cell

The cycling performance of graphite/ $LiNi_{0.5}Mn_{1.5}O_4$ cells at 25 and 55 °C containing electrolyte with or without added lithium alkyl trimethyl borates or lithium aryl trimethyl borates are depicted in Fig. 2. While many different lithium alkyl or aryl trimethyl borates have been prepared and investigated, the cycling performance of the best lithium borates, lithium 4-pyridyl trimethyl borate (LPTB), lithium trimethylsilyl trimethyl borate (LTSTB), lithium propargyl trimethyl borate (LPrTB) and lithium 2-fluorophenyl trimethyl borate (LFPTB) (Scheme 1), are presented in Fig. 2. Upon cycling at room temperature, the capacity retention for all cells containing lithium borate additives is slightly better than that observed for the baseline electrolyte, while the efficiency is comparable. Prolonged cycling of graphite / $LiNi_{0.5}Mn_{1.5}O_4$ cells with the baseline electrolyte is provided in the Supplementary Information (Fig. S2). More significant differences are observed upon cycling the cells at elevated temperature (55 °C) to simulate accelerated aging. After 30 cycles at 55 °C, the cells with baseline electrolyte suffered severe capacity loss, only delivering ~30 % of the initial capacity. The cycling stability of cells was significantly enhanced upon addition 0.5 % (wt.) of any of the lithium borates. However, the best capacity retention (75 %) was observed with LPTB. Since LiBOB has been previously reported as an additive to improve cycling performance of graphite / $LiNi_{0.5}Mn_{1.5}O_4$ cells,[27,39,43] comparative cycling performance of LiBOB to the novel borates has been provided. Cells containing electrolyte with 1.5% LiBOB have 55.9% capacity retention, and lower efficiency than the lithium alkyl or arkyl trimethyl borates. Related charge/ discharge profiles of the cells with and without LPTB for selected cycles are included in the Supplementary Information (Fig. S3a and Fig. S3b). In addition, the cells cycled with electrolyte containing added lithium borates have better efficiency than cells cycled with the baseline electrolyte. The improved efficiency is especially apparent for cells with added LPTB. Cells containing a higher concentration of LPTB (1%) also provide significant improvement, Fig. S4. The improved capacity retention and efficiency suggests the lithium borates may be sacrificially oxidized on the cathode surface to generate a cathode passivation layer, as previously reported for LiBOB.[27] One concern regarding the incorporation of sacrificial additives which modify the surface chemistry of the electrode relates to increased cell impedance leading to poor rate performance and poor low temperature performance. Thus the rate performance and low temperature performance of cells cycled with baseline electrolyte and electrolyte with added LPTB have been investigated and provided in the Supplemental Information (Fig. S5 and Fig. S6). Superior rate performance and enhanced cycling performance at low temperature is observed for cells containing electrolyte with added LPTB. The improved rate and low temperature performance are likely related to changes in the interfacial chemistry of the electrodes. Ex-situ analysis of the electrodes cycled with the baseline electrolyte and electrolyte containing added LPTB is described below.

Anodic/cathode electrochemical behavior of lithium 4-pyridal trimethyl borate

One of the borate additives which provides the best cycling performance is lithium 4-pyridyl trimethyl borate (LPTB). Thus a further investigation LPTB has been conducted. Coin cells (Li/$LiNi_{0.5}Mn_{1.5}O_4$) were prepared with various concentrations of LPTB to investigate the electrochemical behavior on the $LiNi_{0.5}Mn_{1.5}O_4$ cathode. The dQ/dV vs. V profiles are depicted in Fig. 3a, 3b, and 3c. Three pairs of reversible peaks are observed during the charge/discharge processes one pair is

located at 4.0~4.1 V and two peaks are located in the 4.6~4.8 V range, Fig. 3a, corresponding to the redox reactions of Mn^{3+}/Mn^{4+}, $Ni^{2+}/Ni^{3+}/Ni^{4+}$, respectively. The peaks are characteristic of extraction / insertion of lithium cations from / into the $LiNi_{0.5}Mn_{1.5}O_4$ electrode. [27,39,44–46] A slight decrease in the charging potential is observed for the cells with electrolyte containing LPTB compared to the baseline electrolyte, suggesting a decreased polarization of the lithium extraction/insertion process, as shown in Fig. 3c. The decreased polarization can be ascribed to modification of the interfacial chemistry on the cathode electrode upon incorporation of LPTB. A significant difference is observed over the potential range of 4.20~4.45 V during the first charging processes, as shown in the expanded profiles in Fig. 3b. An irreversible oxidative shoulder is present for the cell with electrolyte containing LPTB. The intensity of the oxidation current in the potential range of 4.2~4.45 V increases with an increase in the concentration of LPTB consistent with the oxidative decomposition of LPTB on the cathode surface.

Anodic electrochemical behavior on an inert glass carbon electrode also supports the preferential oxidation of LPTB during the charging process, as shown in Fig. 3d. A significant irreversible oxidative peak is observed at 4.4 V during the first scan. The preferential oxidation of LPTB supports modification of the surface layer formed on the $LiNi_{0.5}Mn_{1.5}O_4$ particles. The surface modification of the cathode particles likely contributes to the enhanced cycling performance presented above. Ex-situ surface analysis of the cycled electrodes has been conducted to better understand the contributions of LPTB to the improved cycling performance, as discussed below.

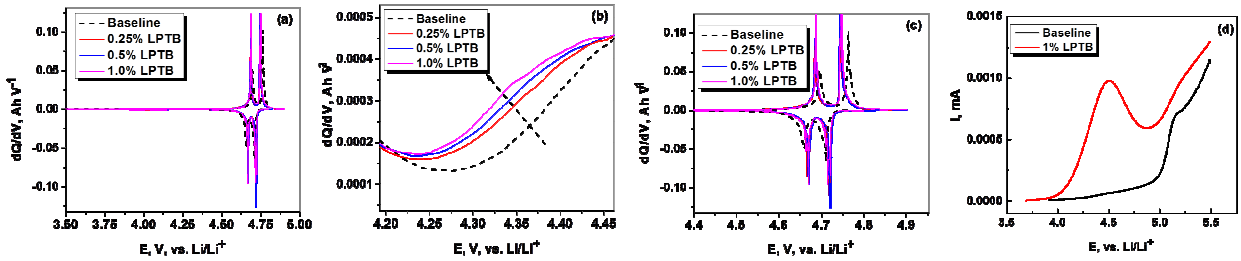

Fig. 3 dQ/dV vs. V profiles of Li/$LiNi_{0.5}Mn_{1.5}O_4$ cells with baseline electrolyte and various concentrations of lithium 4-pyridal trimethyl borate at potential range of 3.5~4.9 V (a), expanded profiles over the potential range 4.2~4.45 V (b), and 4.5~4.9 V (c), and linear sweep voltage profile on glass carbon electrode (d), scan rate 5 mV s^{-1}.

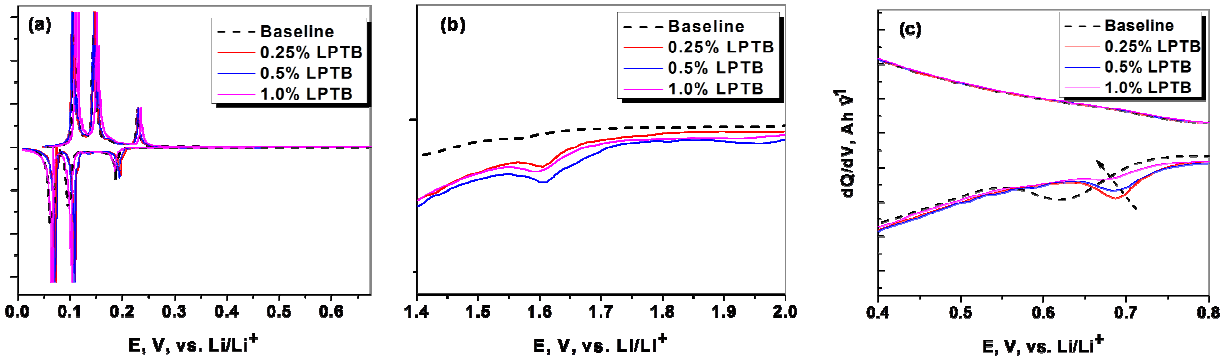

Fig. 4 dQ/dV vs. V profiles of Li/graphite cells with baseline electrolyte and various concentrations of lithium 4-pyridal trimethyl borate at potential range of 0~0.7 V (a), expanded profiles over the potential range 1.4~2.0 V (b), and 0.4~0.8 V (c).

Li/graphite cells with and without LPTB were assembled to investigate the electrochemical reduction process on the graphitic anode. The dQ/dV vs. V profiles for electrolyte with different concentrations of LPTB are depicted in Fig. 4a, 4b, and 4c. Interestingly, incorporation of LPTB results in additional reactivity on the graphitic anode, as evidenced by irreversible reduction peaks at approximately 1.65 V during the first charge, as shown in Fig. 4b. The reaction of LPTB on the surface of the graphitic anode affects the kinetics of the lithium ion intercalation/de-intercalation processes, as shown in Fig. 4a, since the lithium intercalation peaks are shifted to lower potential with increases in the concentration of LPTB consistent with increased interfacial impedance. This suggests that incorporation of LPTB may result in the generation of a more resistive SEI on graphite.

In addition, incorporation of LPTB into the baseline electrolyte modifies the reduction of the bulk electrolyte on the graphitic anode. The results suggest that reduction of LPTB at higher potential (1.65 V) modifies the reduction of bulk electrolyte on the anode electrode during the first charging process. The modification is observed as a shift in the potential of the irreversible electrolyte reduction peak from 0.62 V to 0.68 V followed by a decrease in the intensity of the reduction peak with increase in concentration of LPTB. The unique electrochemical behavior exhibited upon incorporation of LPTB likely contributes to the enhanced cycling performance of graphite/$LiNi_{0.5}Mn_{1.5}O_4$ cells upon cycling at high voltage and elevated temperature. In order to obtain a better understanding of the reactivity of LPTB both on anode and cathode, ex-situ surface analysis of the cycled electrodes has been conducted as described below.

FE-SEM images and TEM of cathodes

The FE-SEM images of the $LiNi_{0.5}Mn_{1.5}O_4$ cathodes, fresh and after cycling both at 25 and 55 ^{o}C are provided in Fig. 5. The fresh electrode consists of secondary spherical particles with diameter of 5~10 µm, Fig. 5a. The secondary spherical particles are made up of primary particles around a hundred nanometers in length, Fig. 5d, and 5g. After cycling with baseline electrolyte at 55 ^{o}C, the bulk structure of the secondary particle is damaged and broken down to smaller particles with sharp edges. The magnified SEM images, Fig. 5e and Fig. 5h, clearly show damage of the primary particles as

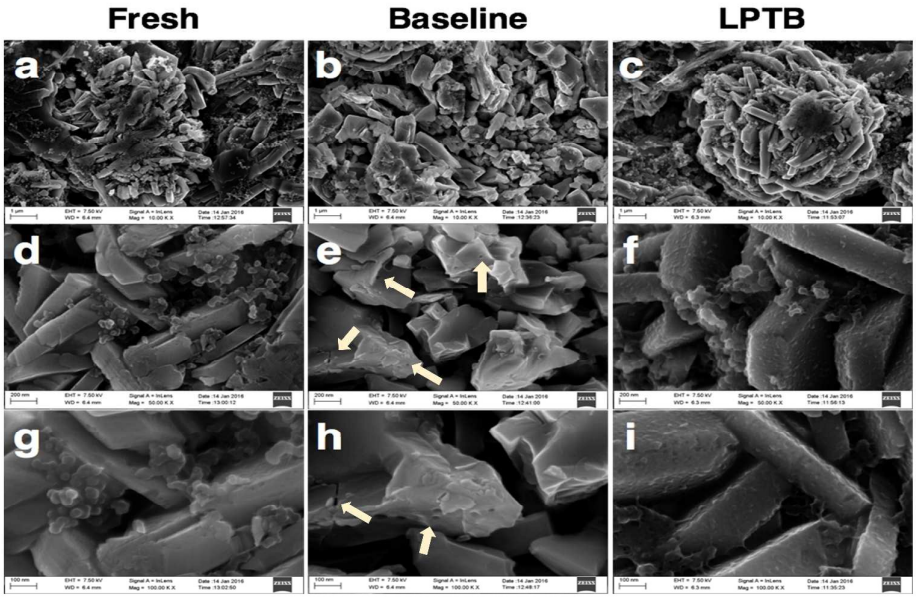

Fig. 5 FE-SEM images of the $LiNi_{0.5}Mn_{1.5}O_4$ cathodes, fresh (a), cycled electrode with baseline electrolyte (b), and cycled electrode with 0.5% added lithium 4-pyridyl trimethyl borate (LPTB), and corresponding higher magnifications, fresh (d, g), baseline (e, h), and added LPTB (f, i), respectively.

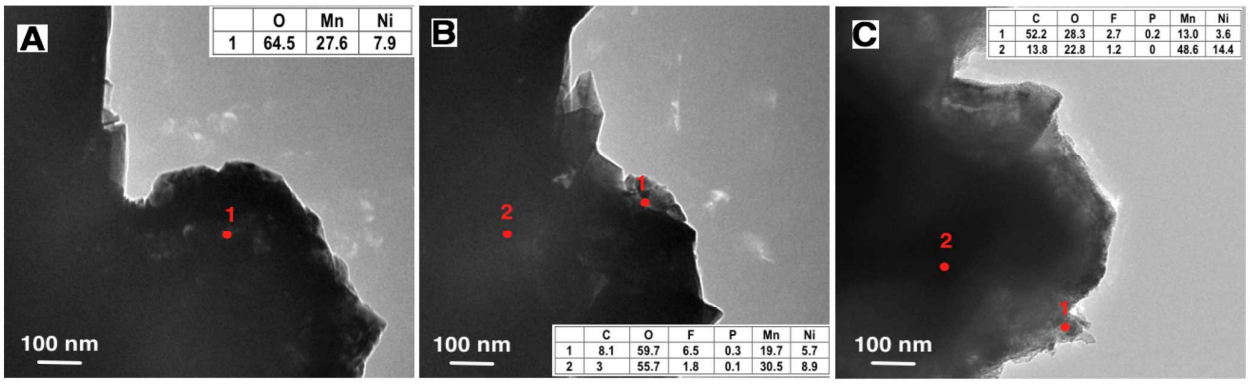

Fig. 6 TEM bright-field images and elemental concentration of the fresh $LiNi_{0.5}Mn_{1.5}O_4$ (A), after cycling at both 25 and 55 ^{o}C in baseline electrolyte (B), and after cycling at both 25 and 55 ^{o}C in LPTB containing electrolyte (C).

highlighted with arrows, consistent with etching and pitting of the electrode cycled with baseline electrolyte. Surprisingly, no surface layer or precipitates are observed on the surface of the particles. The etching is likely due to the dissolution of Mn or Ni upon cycling at high voltage and elevated temperature, as previously reported.[37]

However, the integrity of both the secondary and primary particles are maintained after cycling at 55°C for the LPTB containing electrolyte. No evidence of cracks or pitting are observed, as shown in Fig. 5c, 5f, and 5i. The surface of the primary particles are covered with a thin coating, which most likely results from the decomposition of LPTB on the surface. Further evidence supporting this hypothesis is provided from XPS and TEM results discussed below.

The TEM images and elemental concentrations of the fresh cathode and cathodes cycled with baseline electrolyte with and without LPTB are provided in Fig. 6. The surface of fresh $LiNi_{0.5}Mn_{1.5}O_4$ particle has no surface film, as shown in Fig. 6A. The EDX analysis of the bulk particle suggests that the predominant elements are O, Mn, and Ni with concentrations of 64.5, 27.6, and 7.9 %, respectively. After cycling at 25 ^{o}C and 55 ^{o}C with the baseline electrolyte, the surface of the cathode particles is modified and thin deposits corresponding to electrolyte oxidation products are observed on the edges (Fig. 6B). The thickness of the surface layer is very thin, less than 20 nm. Significant decreases in the elemental concentration of Mn and Ni (spot 1) are observed on the surface, which can be ascribed to the electrode surface covered by the decomposition products of the electrolyte or transition metal dissolution from the metal oxide. Increases in the concentration of C, F, and P further support that a surface layer is formed on the edges of the cathode particles from the decomposition of the electrolyte, $LiPF_6$ and carbonate solvents.[27] Incorporation of LPTB into the electrolyte results in the generation of a thinner and more uniform cathode surface film after cycling (Fig. 6C).

X-ray photoelectron spectroscopy (XPS) of the $LiNi_{0.5}Mn_{1.5}O_4$ cathodes

In order to better understand the changes to the surfaces, XPS spectra were acquired of the fresh cathode and cathodes extracted from graphite/$LiNi_{0.5}Mn_{1.5}O_4$ cells after cycling at both room temperature and elevated temperature with and without added LPTB (Fig. 7). The elemental concentrations of the fresh $LiNi_{0.5}Mn_{1.5}O_4$, after cycling both at 25 ^{o}C and 55 ^{o}C with baseline electrolyte and electrolyte with 0.5% LPTB, are provided in Table 1. The fresh electrode has a high concentration of Mn, Ni, and O from the metal oxide and a high concentration of C and F from the PVDF binder. After cycling with the baseline electrolyte, the concentrations of C, F, Mn, and Ni are decreased; while O and P are increased, suggesting the formation of a surface film composed of electrolyte decomposition products. The changes to the atomic concentrations of the electrode surface are different for the electrode cycled with electrolyte containing added LPTB. While the concentrations of Mn, Ni, and C are deceased, the decrease in the concentrations of Mn and Ni are much less than that observed for the baseline electrolyte while the decrease in the concentration of C is much more. Increases in the concentrations of F, O, P and B are also observed. The higher concentrations of Mn and Ni suggest that the surface

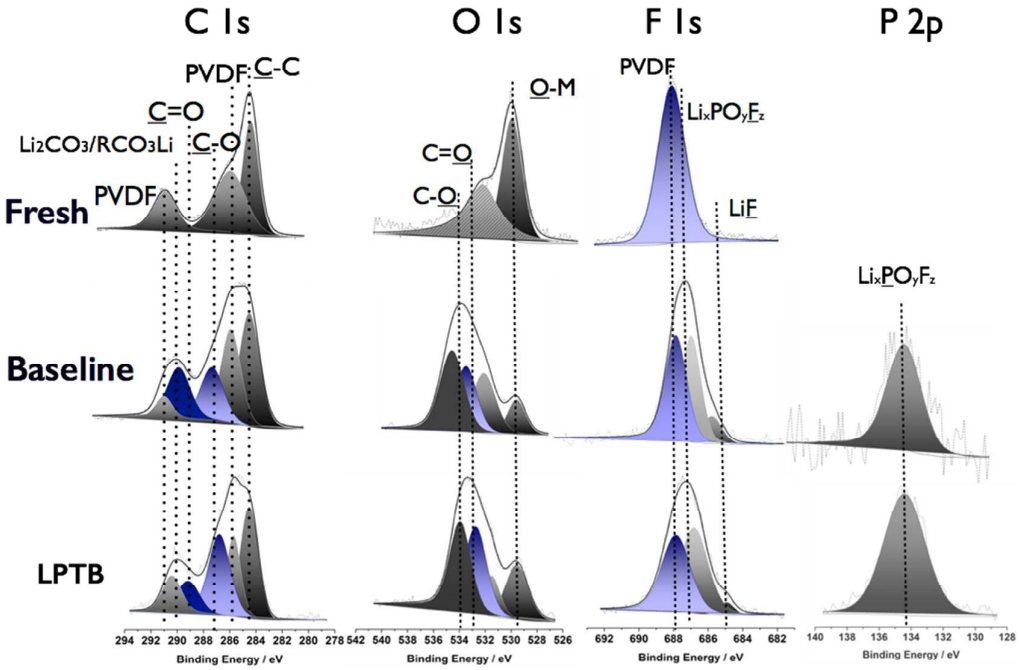

Fig. 7 C 1s, O 1s, F 1s, and P 2p XPS spectra of the $LiNi_{0.5}Mn_{1.5}O_4$ cathode, fresh, and after cycling at elevated temperature with and without 1% LPTB additive.

Table 1 Elemental concentration of $LiNi_{0.5}Mn_{1.5}O_4$ cathode surface as determined by XPS.

	C 1s (%)	O 1s (%)	F 1s (%)	P 2p (%)	Mn 2p (%)	Ni 2p (%)	B 1s (%)
Fresh	69.2	7.9	14.9		4.2	3.8	
Baseline	65.1	16.7	12.7	1.2	1.5	2.8	
LPTB	46.6	22.7	16.7	1.6	3.6	3.1	5.7

film is thinner than the surface film generated with the standard electrolyte while the presence of B and high concentration of O suggests that the surface film is rich in borates.

The C 1s spectrum of the fresh $LiNi_{0.5}Mn_{1.5}O_4$ cathode contains three peaks, 284.3, 285.7, and 290.4 eV, corresponding to the conductive carbon, PVDF binder (C-H), and PVDF binder (C-F), respectively. XPS spectra of B 1s, Mn 2p, and Ni 2p are provided in the Supplementary Information (Fig. S7). A single peak characteristic of PVDF is observed in the F 1s spectrum at 687.6 eV. The O 1s spectrum of the fresh $LiNi_{0.5}Mn_{1.5}O_4$ cathode is dominated by transition metal oxide (~529.5 eV), and contains a low concentration of Li_2CO_3 (531.5 eV), which is frequently present on fresh cathode particles.[48]

The XPS spectra of the cathodes after cycling with the baseline electrolyte are consistent with the presence of electrolyte decomposition products on the cathode surface. New peaks are observed in the C 1s spectrum at 286 and 290 eV consistent with the presence of –CO and $–CO_3$ containing species, respectively. Corresponding new peaks are observed in the O 1s spectrum at 533-534 and 532-533 eV consistent with the presence of C-O and C=O containing species. The F1s spectrum has a new peak at 685 eV consistent with the presence of LiF.[49,50] A small peak is observed in the P2p spectrum at 134.5 eV characteristic of $Li_xPO_yF_z$. The F1s peak for $Li_xPO_yF_z$ overlaps with the peak for the PVDF binder at 687.6 eV. The peak for the metal oxide at 529.5 eV is diminished relative to the fresh electrode consistent with the formation of a thin surface layer on the cathode.

Analysis of the cathodes cycled with electrolyte containing added LPTB reveal the presence of similar peaks in the XPS spectra. However, the peak for the metal oxide has greater intensity than is observed for the cathode cycled with the baseline electrolyte suggesting the surface film is thinner on the electrode cycled with electrolyte containing LPTB. In addition, a single new peak is observed in the B1s spectrum at 192 eV consistent with the presence of borates suggesting that LTMB is involved in the cathode film forming process generating high concentrations of B-O containing species on the cathode surface. This is consistent with the electrochemical behavior observed in cyclic voltammetry profiles described above.

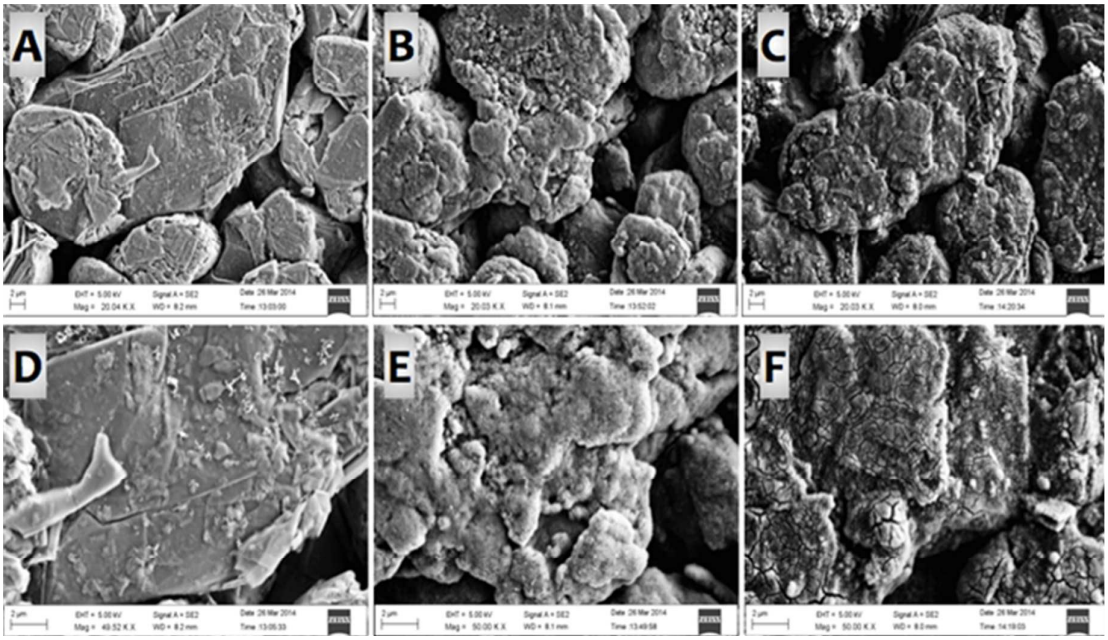

Fig. 8 FE-SEM images of the CPG graphite, fresh (A), cycled electrode with baseline electrolyte (B), and cycled electrode with 0.5% lithium 4-pyridyl trimethyl borate (LPTB) added electrolyte (C), and corresponded higher magnifications, fresh (D), baseline (E), and LPTB (F), respectively.

FE-SEM images and TEM of anodes

The FE-SEM images of the CPG graphite, fresh and cycled with various electrolytes are provided in Fig. 8. The fresh CPG graphite electrode has a smooth surface and sharp edges, as shown in Fig. 8A and 8D. After cycling, significant changes to the graphite surface are observed for electrodes cycled with both the baseline electrolyte and electrolyte with added LPTB. Non-uniform amorphous deposits are observed on the surface of the graphite electrode cycled with the baseline electrolyte. The changes are characteristic of electrolyte decomposition and SEI formation. However, the electrolyte decomposition products are thinner and grainier on the surface of the graphite electrode cycled with electrolyte containing added LPTB, as shown in Fig. 8C and 8F. The significant difference is likely caused by the presence of LPTB, which participates in the SEI formation process changing the chemistry, structure, and

morphology of the surface layer, which is consistent with the modified electrochemical behavior on the anode electrode as discussed above.

The TEM images and elemental concentrations determined by EDX of CPG graphite, fresh and after cycling with and without added LPTB are depicted in Fig. 9. The edges of the fresh graphite particles are sharp and clean, as shown in Fig. 9A. The elemental composition is dominated by C with a low concentration of O. After cycling, decomposition of the electrolytes results in the appearance of an SEI on the edges of the graphite particles from electrodes cycled with both the baseline electrolyte and the electrolyte with added LPTB. The SEI is thicker on the edges of the graphite particles cycled with the baseline electrolyte (40-100 nm) compared to the electrode cycled with the electrolyte containing added LPTB (10-20 nm). Two different locations of the cycled anodes were analyzed by EDX, edge and bulk, as depicted in the inset tables of Fig. 9. The concentrations of O, F, and P are higher at the edge than the bulk of the particle, consistent with the presence of an SEI generated from the decomposition products of the electrolyte. Low concentrations of Mn and Ni are detected on the edge of the electrode cycled with the baseline consistent with transition metal dissolution from the cathode as previously reported.[37] The concentration of transition metals is significantly lower on the surface of the anode cycled with electrolyte containing added LPTB suggesting that incorporation of LPTB inhibits transition metal dissolution from the cathode. A similar inhibition of transition metal dissolution has been reported for electrolytes containing added LiBOB.[27]

X-ray photoelectron spectroscopy (XPS) of the graphite anodes

The graphite electrodes were further analyzed via XPS. The XPS spectra of the graphite anodes, fresh and after cycling with baseline electrolyte and electrolyte with added LPTB are depicted in Fig. 10. The elemental concentrations, as determined by XPS, are provided in Tab. 2. After cycling, the concentration of C is dramatically decreased for both electrolytes; while the concentrations of O, F, and P are increased consistent with the formation of an SEI.

The XPS spectra of the graphite anodes, fresh and after cycling with baseline electrolyte and electrolyte with added LPTB are depicted in Fig. 10. The elemental concentrations, as determined by XPS, are provided in Tab. 2. After cycling, the concentration of C is dramatically decreased for both electrolytes; while the concentrations of O, F, and P are increased consistent with the formation of an SEI. In addition, a significant concentration of B is observed on the electrode cycled with electrolyte containing added LPTB, consistent with reduction of LPTB on the anode surface and modification of the SEI.

The C 1s spectrum of the fresh graphite consists of two peaks. The peak at 284.3 eV is assigned to graphite and the peak at 286.5 eV corresponds to the CMC binder (C-O bond). The corresponding C-O peak is observed in the O 1s spectrum at 533.4 eV. Analysis of the graphite anode after cycling with the baseline electrolyte reveals new species in the C 1s, O 1s, F 1s, and P 2p XPS spectra characteristic of electrolyte decomposition products on the electrode surface. In addition to the peaks present on the fresh anode, new peaks consistent with C-O (~286 eV) and Li_2CO_3 or $ROCO_2Li$ (290 eV) containing species are present in the C 1s spectrum of the graphite anode. The corresponding peaks for C=O (532~533 eV), and C-O (533~534 eV) containing species are observed in the O 1s XPS spectrum.[49,50] The C1s and O1s spectra are consistent with the presence of lithium alkyl carbonates and Li_2CO_3 on the surface of the cycled graphite anodes which are common decomposition products of EC/$LiPF_6$ based electrolyte.[51] Two peaks are observed in the F 1s spectrum, LiF (684.5 eV) and $Li_xPO_yF_z$ (~686 eV). The corresponding peak for $Li_xPO_yF_z$ is observed in the P 2p spectrum, ~134.5 eV.

Similar changes to the XPS spectra are observed for graphite anodes cycled with electrolyte with added LPTB. The XPS spectra are consistent with the presence of lithium alkyl carbonates, LiF, Li_2CO_3, and $Li_xPO_yF_z$,, as described above with the baseline electrolyte (Fig. 10). However, the relative concentration of C is significantly decreased from 66.5 % to 45.8 % and the relative concentration of O is increased from 11.2 % to 27.9 % (Table 2), suggesting that more oxygen containing degradation products are generated on the anode surface for the LPTB containing electrolyte, which is most likely due to the participation of LPTB in the SEI formation process. A single B peak is observed in the B 1s XPS spectrum at 192 eV suggesting that LPTB is involved in the SEI formation process. This is consistent with the dQ/dV profiles of the Li/graphite cells during the first charge/discharge process as discussed above (Fig. 4). In addition, a Mn 3p peak is present on the electrode cycled with the baseline electrolyte; while it is absent from the electrode cycled with the LPTB containing electrolyte, suggesting that LPTB inhibits Mn dissolution from the cathode and deposition of Mn on the anode.

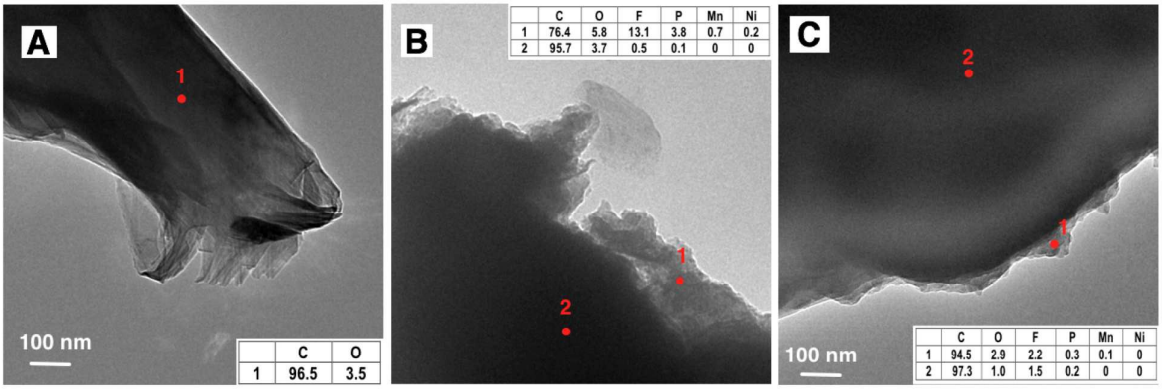

Fig. 9 TEM bright-field images and elemental concentrations of the fresh CPG graphite (A), after cycling at both 25 and 55 °C in baseline electrolyte, and after cycling at both 25 and 55 °C in LPTB containing electrolyte.

Table 2 Elemental concentration of graphite anode surface as determined by XPS

	C 1s (%)	O 1s (%)	F 1s (%)	P 2p (%)	B 1s (%)	Mn 3s (%)
Fresh	89.4	10.6				
Baseline	66.5	11.2	16.9	2.9		2.5
LPTB	45.8	27.9	13.3	3.1	9.9	

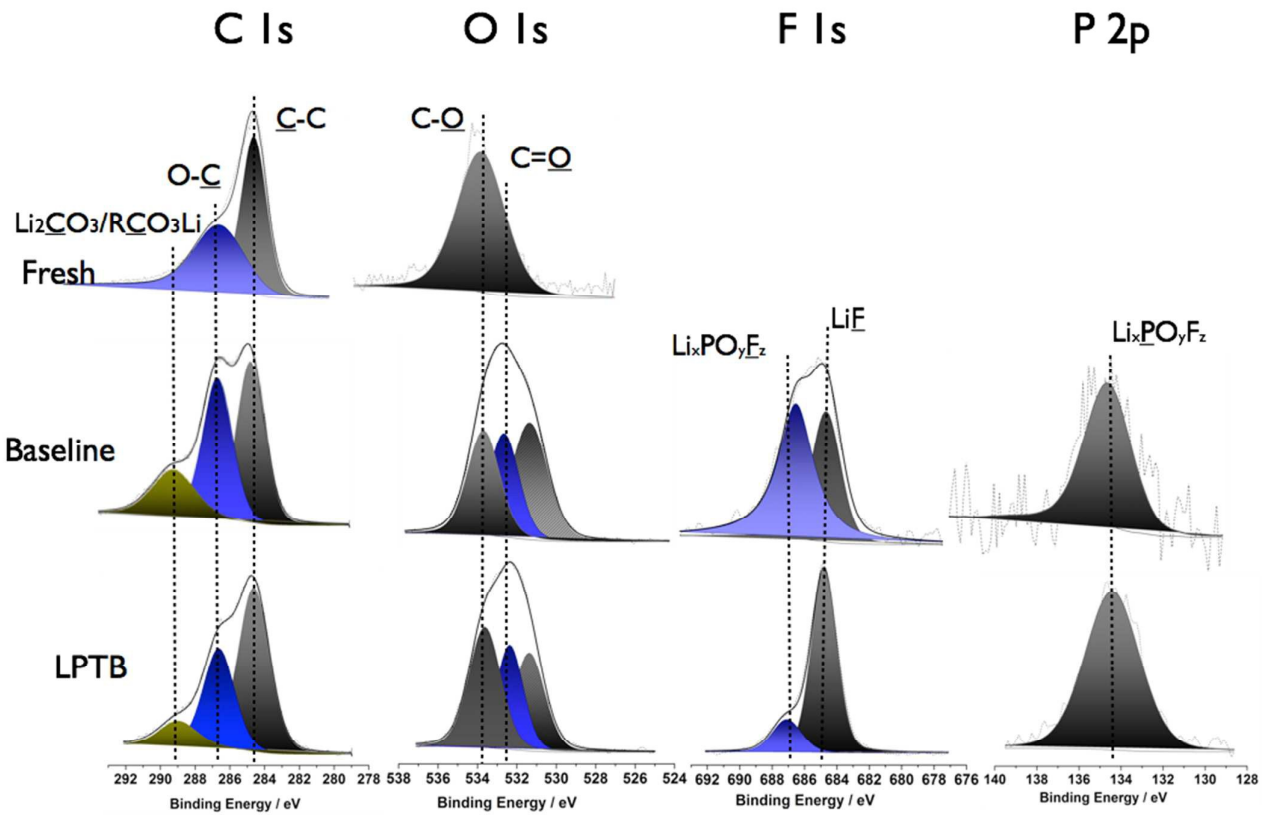

Fig. 10 C 1s, O 1s, F 1s, and P 2p XPS spectra of the graphite electrode, fresh, and after cycling at elevated temperature with and without 0.5% lithium 4-pyridyl trimethyl borate (LPTB).

Conclusions

A series of lithium organoborate additives have been prepared and investigated as cathode film forming additives for high voltage $LiNi_{0.5}Mn_{1.5}O_4$ cathodes for lithium ion batteries. The additives are prepared via the reaction of lithium alkoxides or lithium phenoxides with trimethyl borate to generate lithium alkyl trimethyl borates and lithium aryl trimethyl borates. The compounds are prepared in high yield and purity. Incorporation of the lithium organoborate additives into 1.0 M $LiPF_6$ in EC/EMC results in improved capacity retention and efficiency for graphite / $LiNi_{0.5}Mn_{1.5}O_4$ cells. The largest performance enhancements are observed for electrolyte containing lithium 4-pyridyl trimethyl borate (LPTB). Reaction of LPTB on the surface of the cathode and anode is supported by dQ/dV profiles and linear sweep voltammetry. Upon charging the anionic organo borates are polarized toward the cathode where they oxidatively decompose. Modification of the organic functional group on the lithium alkyl trimethyl borates and lithium aryl trimethyl borates allows control over the structure of the cathode surface film. In order to develop a better understanding of the source of the performance enhancement for cells containing added LPTB, ex-situ surface analysis via TEM, SEM, XPS and IR-ATR has been conducted on the cycled electrodes. The ex-situ surface analysis provides additional support for the reaction of LPTB on the surface of both the cathode and the anode and modification of the surface films. Incorporation of LPTB results in the generation of a borate rich passivation layer on the cathode which inhibits electrolyte oxidation on the surface of the cathode. The mechanism is likely analogous to that previously reported for the reaction of tetraborate with pyrite (Scheme 2).[52] The tetraalkyl borate is oxidized by the metal oxide surface to irreversibly generate a metal oxide borate complex. Complex formation is likely to occur at the most reactive sites on the surface of the metal oxide thus inhibiting electrolyte oxidation. We are currently conducting a more detailed investigation of this reaction to better understand the mechanism of surface modification and the structure of the novel surface film. In addition, incorporation of LPTB inhibits Mn and Ni dissolution from the cathode and subsequent deposition on the anode. The inhibition of transition metal dissolution inhibits damage to the anode SEI which likely contributes to the improved electrochemical performance.

Scheme 2

$$M_xO_y + B(OR)_4^- \xrightarrow{-e^-} M_xO_y\text{-}B(OR)_4$$

Acknowledgements

The authors thank BASF SE Electrochemistry Research Network for financial support.

Notes and references

1 H.-G. Jung, M. W. Jang, J. Hassoun, Y.-K. Sun and B. Scrosati, *Nat. Commun*, 2011, **2**, 516.
2 B. Dunn, H. Kamath and J.-M. Tarascon, *Science*, 2011, **334**, 928–35.
3 A. Manthiram, *J. Phys. Chem. Lett*., 2011, **2**, 176–184.
4 M. Pivko, M. Bele, E. Tchernychova, Z. Logar, R. Dominko and M. Gaberscek, *Chem. Mater*., 2012, **24**, 1041–1047.
5 X. Rui, X. Zhao, Z. Lu, H. Tan, D. Sim, H. H. Hng, R. Yazami, T. M. Lim and Q. Yan, *ACS Nano*, 2013, **7**, 5637–46.
6 Y. Cao, J. Duan, G. Hu, F. Jiang, Z. Peng, K. Du and H. Guo, *Electrochim. Acta*, 2013, **98**, 183–189.
7 G. Hautier, A. Jain, S. P. Ong, B. Kang, C. Moore, R. Doe and G. Ceder, *Chem. Mater*., 2011, **23**, 3495–3508.
8 J. Yu, K. M. Rosso and J. Liu, *J. Phys. Chem. C*, 2011, **115**, 25001–25006.
9 C. A. J. Fisher, V. M. H. Prieto and M. S. Islam, *Chem. Mater*., 2008, **20**, 5907–5915.
10 J. Ni, H. Wang, L. Gao and L. Lu, *Electrochim. Acta*, 2012, **70**, 349–354.
11 D.-W. Han, Y.-M. Kang, R.-Z. Yin, M.-S. Song and H.-S. Kwon, *Electrochem. commun*., 2009, **11**, 137–140.
12 J. L. Allen, T. R. Jow and J. Wolfenstine, *J. Power Sources*, 2011, **196**, 8656–8661.
13 J. Liu and a. Manthiram, *J. Electrochem. Soc*., 2009, **156**, A833-A838.
14 J. Liu and A. Manthiram, *J. Phys. Chem. C*, 2009, **113**, 1695–1707.
15 D. Aurbach, B. Markovsky, Y. Talyossef, G. Salitra, H.-J. Kim and S. Choi, *J. Power Sources*, 2006, **162**, 780–789.
16 X. Zhang, F. Cheng, J. Yang and J. Chen, *Nano Lett*., 2013, **13**, 2822–2825.
17 Z. Zhang, L. Hu, H. Wu, W. Weng, M. Koh, P. C. Redfern, L. a. Curtiss and K. Amine, *Energy Environ. Sci*., 2013, **6**, 1806-1810.
18 L. Yang, B. Ravdel and B. L. Lucht, Electrochem. *Solid-State Lett.*, 2010, **13**, A95-A97.
19 J. Wolfenstine and J. Allen, *J. Power Sources*, 2005, **142**, 385–390.
20 J. A. Read, A. V Cresce, M. H. Ervin and K. Xu, *Energy Environ. Sci.*, 2014, **7**, 617–620.
21 J. Liu and a. Manthiram, *J. Electrochem. Soc*., 2009, **156**, A66-A72.
22 A. Manthiram, K. Chemelewski and E.-S. Lee, *Energy Environ. Sci.*, 2014, **7**, 1339–1350.
23 Y.-S. Kang, T. Yoon, J. Mun, M. S. Park, I.-Y. Song, A. Benayad and S. M. Oh, *J. Mater. Chem. A*, 2014, **2**, 14628-14633.
24 Y.-M. Song, J.-G. Han, S. Park, K. T. Lee and N.-S. Choi, *J. Mater. Chem. A*, 2014, **2**, 9506-9513.
25 N. P. W. Pieczonka, L. Yang, M. P. Balogh, B. R. Powell, K. Chemelewski, A. Manthiram, S. a. Krachkovskiy, G. R. Goward, M. Liu and J.-H. Kim, *J. Phys. Chem. C*, 2013, **117**, 22603–22612.
26 H. Bouayad, Z. Wang, N. Dupre and R. Dedryve, *J. Phys. Chem. C*, 2014, **118**, 4634–4648.
27 M. Xu, L. Zhou, Y. Dong, Y. Chen, a. Garsuch and B. L. Lucht, *J. Electrochem. Soc.*, 2013, **160**, A2005–A2013.
28 L. Yang and B. L. Lucht, *Electrochem. Solid-State Lett*., 2009, **12**, A229-A231.
29 L. Yang, T. Markmaitree and B. L. Lucht, *J. Power Sources*, 2011, **196**, 2251–2254.
30 S. Dalavi, M. Xu, B. Knight and B. L. Lucht, *Electrochem. Solid-State Lett.*, 2011, **15**, A28–A31.
31 S. Li, W. Zhao, X. Cui, Y. Zhao, B. Li, H. Zhang, Y. Li, G. Li, X. Ye and Y. Luo, *Electrochim. Acta*, 2013, **91**, 282–292.
32 A. von Cresce and K. Xu, *J. Electrochem. Soc*., 2011, **158**, A337–A342.
33 B. Zhang, M. Metzger, S. Solchenbach, M. Payne, S. Meini, H. A. Gasteiger, A. Garsuch and B. L. Lucht, J. Phys. Chem. C, 2015, 119, 11337–11348.
34 M. Q. Xu, W. S. Li, X. X. Zuo, J. S. Liu and X. Xu, *J. Power Sources*, 2007, **174**, 705–710.
35 D. Aurbach, K. Gamolsky, B. Markovsky, Y. Gofer, M. Schmidt and U. Heider, *Electrochim. Acta*, 2002, **47**, 1423–1439.
36 J.-H. Kim, N. P. W. Pieczonka and L. Yang, *Chemphychem*, 2014, **15**, 1940–54.

37 D. Lu, M. Xu, L. Zhou, a. Garsuch and B. L. Lucht, *J. Electrochem. Soc.*, 2013, **160**, A3138–A3143.
38 C. L. Campion, W. Li and B. L. Lucht, *J. Electrochem. Soc*., 2005, **152**, A2327–A2334.
39 M. Xu, N. Tsiouvaras, A. Garsuch, H. A. Gasteiger and B. L. Lucht, *J. Phys. Chem. C*, 2014, **118**, 7763–7368.
40 J. Vatamanu, O. Borodin and G. D. Smith, *J. Phys. Chem. C*, 2012, **116**, 1114–1121.
41 W. Li and B. L. Lucht, *J. Power Sources*, 2007, **168**, 258–264.
42 W. Li, C. Campion, B. L. Lucht, B. Ravdel, J. DiCarlo and K. M. Abraham, *J. Electrochem. Soc*., 2005, **152**, A1361–A1365.
43 X. Fang, M. Ge, J. Rong and C. Zhou, *J. Mater. Chem. A*, 2013, **1**, 4083-4088.
44 Y. Xue, Z. Wang, F. Yu, Y. Zhang and G. Yin, *J. Mater. Chem. A*, 2014, *2*, 4185-4191.
45 H. B. Lin, Y. M. Zhang, H. B. Rong, S. W. Mai, J. N. Hu, Y. H. Liao, L. D. Xing, M. Q. Xu, X. P. Li and W. S. Li, *J. Mater. Chem. A*, 2014, **2**, 11987-11995.
46 Y. -K, Sun, K.-J. Hong, P. Jai and K. Amine, *Electrochem. commun.*, 2002, **4**, 344–348.
47 W. Li and B. L. Lucht, *J. Electrochem. Soc*., 2006, **153**, A1617.
48 P. Niehoff, S. Passerini and M. Winter, *Langmuir*, 2013, **29**, 5806–5816.
49 A. v Cresce, S. M. Russell, D. R. Baker, K. J. Gaskell and K. Xu, *Nano Lett.*, 2014, **14**, 1405–12.
50 M. Nie, D. Chalasani, D. P. Abraham, Y. Chen, A. Bose and B. L. Lucht, *J. Phys. Chem. C*, 2013, **117**, 1257–1267.
51 X. –H. Wang, *J. Colloid and Interface Science*, 1996, **178**, 628-637.

Broader Context

Lithium ion batteries are widely used in consumer electronics and use is rapidly expanding in electric vehicles. However, for both of these applications there is significant demand for greater energy density. One method to increase the energy density of lithium ion batteries is to increase the voltage of the cathode. The instability of standard carbonate electrolytes at high voltage significantly limits the implementation of high voltage cathodes (>4.5 V vs Li/Li^+). In this report, a novel method to improve the stability of high voltage cathodes is presented. The novel electrolyte system utilizes Additives for Designed Surface Modification (ADSM) to generate a cathode passivation layer similar in nature to the Solid Electrolyte Interphase (SEI) on the anode. A series of lithium alkyl trimethyl borates and lithium aryl trimethyl borates have been prepared and investigated in graphite / $LiNi_{0.5}Mn_{1.5}O_4$ cells. The lithium borates act as functional group delivery agents to generate a functionalized borate rich passivation layer which improves the capacity retention and efficiency of graphite / $LiNi_{0.5}Mn_{1.5}O_4$ cells.